# Correlation-function hierarchies in nonlinear quantum optics

C. J. Mertens, J. M. Hasty, H. H. Roark III, D. Nowakowski,* and T. A. B. Kennedy
*School of Physics, Georgia Institute of Technology, Atlanta, Georgia 30332*
(Received 23 January 1995)

A correlation-function hierarchy for intracavity quantum optical systems has been derived using nonequilibrium Green function methods. A specific truncation is applied to study nonlinear quantum fluctuations in an optical parametric oscillator near threshold. An analysis of the limitations of the truncation and comparison of its efficiency and accuracy relative to coherent state phase space methods and wave-function simulation methods is made.

PACS number(s): 42.50.Lc, 42.50.Dv, 05.30.Jp, 42.65.Ky

## I. INTRODUCTION

Quantum noise becomes an increasingly important factor in the physics of dissipative optical systems as the system size is scaled down. The issue of system size, as measured by characteristic scales of photon or particle number, is therefore central to the physics of miniaturized devices, for example, low threshold parametric oscillators [1] or cavity quantum electrodynamic (QED) lasers [2,3]. The basic reason is readily understood from the following argument. The rms electric field of a single photon state increases as the mode volume is reduced, and thus the electric-field strength required to turn on a nonlinear effect involves fewer and fewer photons in this limit, provided the photon lifetime is kept constant.

In small systems, operation is strongly influenced by quantum fluctuations whose magnitude depends on the characteristic scales. Associated with this regime is the long standing theoretical problem of how to extract dynamical information outside the application of linearization theory in which dynamical correlations are independent of system-size scales [4,5]. In previous works [6,7] we have argued that an approach based on a truncated hierarchy of photon Green functions has both conceptual and practical advantages for this kind of problem. The one- and two-photon Green functions themselves are directly related to certain dynamical correlations measured by standard photodetection procedures.

In this paper we study system-size effects in a degenerate optical parametric oscillator (OPO), using an improved version of our previous theory [6]. The principal improvement is the inclusion of quantum corrections to the classical intracavity mean fields, although anomalous multiphoton polarization processes are also included. We are primarily concerned with practical application of the method, a careful assessment of the accuracy of the bare-vertex approximation employed to truncate the hierarchy, and comparisons with alternative standard quantum optical methods for dissipative systems where feasible [8,9]. In this regard we note that one should expect direct correlation-function methods to be efficient for practical calculations since they discard extraneous information contained in the density matrix, or stochastic wave-function approaches. The OPO problem considered is, apart from its physical interest, a powerful test of the approach in that it involves two quantized field modes and thus rules out density matrix photon number expansion methods, unless one operates in the extreme quantum limit of a few photons, far from the domain of current experiments [10], or one employs a purely numerical course involving supercomputers and sparse matrix storage techniques [11].

We consider the OPO in the regime just below the classical threshold. The theoretical model is described by the OPO master equation given in Ref. [8], in the rotating frame with both modes at resonance

$$\frac{d\rho}{dt} = \frac{\kappa}{2}[a_1^\dagger a_2 - a_2^\dagger a_1^2, \rho] + E_2[a_2^\dagger - a_2, \rho] + \sum_{k=1}^{2} \gamma_k \{2a_k \rho\, a_k^\dagger - a_k^\dagger a_k \rho - \rho\, a_k^\dagger a_k\}, \tag{1.1}$$

where $\rho$ is the density matrix, $a_k$ and $a_k^\dagger$ $(k = 1, 2)$ are annihilation and creation operators for the subharmonic (mode 1) and pump (mode 2) modes, $\kappa$ is the nonlinear coupling constant, $E_2$ is the pump driving field, and $\gamma_k$ $(k = 1, 2)$ are the mode damping rates. Below threshold the subharmonic has zero mean value and the pump, which is driven by the external field $E_2$, has classical amplitude $\alpha_2$ determined by the steady-state classical equations. A unitary transformation with the coherent-state displacement operator $D(\alpha_2)$ is performed on (1.1), using $[D(\alpha_2)]^\dagger a_2 D(\alpha_2) = a_2 + \alpha_2$, so that the subharmonic and pump annihilation operator represent the quantum corrections to their respective classical values in the vacuum picture. The transformed master equation is given by

$$\frac{d\hat{\rho}}{d\tau} = \frac{1}{i\hbar}[H, \hat{\rho}] + \sum_{k=1}^{2} \frac{\gamma_k}{\gamma_1} \{2a_k \hat{\rho} a_k^\dagger - a_k^\dagger a_k \hat{\rho} - \hat{\rho} a_k^\dagger a_k\}, \tag{1.2}$$

*Present address: Department of Physics, Harvard University, Cambridge, MA 02138.

 

where $\hat{\rho}$ is the transformed density operator, $\tau = \gamma_1 t$ is time measured in units of the inverse damping rate $\gamma_1^{-1}$ of the subharmonic mode, and the Hamiltonian is given by

$$H = i\hbar\frac{p}{2}[a_1^{\dagger 2} - a_1^2] + \frac{i\hbar}{2\sqrt{n_{\rm th}}}[a_1^{\dagger 2}a_2 - a_1^2 a_2^\dagger]. \qquad (1.3)$$

The device is governed by three parameters (the notation follows that of our earlier works [6,7]): $\gamma = \gamma_2/\gamma_1$, the ratio of the cavity decay rates for pump (mode 2) and subharmonic (mode 1), which have frequencies $\omega_2$ and $\omega_1$, respectively, with $\omega_2 = 2\omega_1$; $p$, the dimensionless classical pump amplitude scaled so that $p = 1$ corresponds to the classical threshold; $n_{\rm th}$, the pump photon number at threshold $p = 1$. System-size effects are increasingly important as $n_{\rm th}$ is reduced, i.e., for large nonlinearities and small mode volumes, particularly as the classical threshold is approached. In terms of the parameters in (1.1), $p = \kappa E_2/\gamma_1\gamma_2$ and $n_{\rm th} = (\gamma_1/\kappa)^2$. At threshold linearized theory spuriously predicts divergent quadrature fluctuations and perfect squeezing of the two subharmonic quadratures, respectively [12].

The remainder of the paper is organized as follows. In Sec. II we outline the basic elements of the Green function theory and present the truncated hierarchy in the bare-vertex approximation. In Sec. III we derive some approximate analytical expressions and recover results previously found by Plimak and Walls [13], which provide considerable insight into the nature of quantum noise below the threshold where "condensation" of the subharmonic is achieved. In Sec. IV we present an analytic criterion on the limits of validity of the bare vertex approximation, and an approximate expression for the bare vertex system-size expansion parameter. In Sec. V we make explicit comparisons of stationary observables and dynamical correlations using the analytical approximations of Sec. III, the complex $P$ distribution, and the wave-function simulation method (see the Appendix). Our conclusions are summarized at the end.

## II. THEORY

### A. Green function equations

The quantum field theoretic approach provides a hierarchy of equations for correlation functions in the form of Dyson equations [14]. In practice these must be truncated in a physically reasonable way, taking into account the most significant dynamical processes. In an earlier paper [6] the authors derived Dyson equations for the OPO using a diagrammatic method, and considered a specific truncation: the so-called *bare-vertex approximation* — the vertex part is truncated at zeroth order in the inverse of the threshold pump photon number, $n_{\rm th}$. The earlier analysis was limited in that renormalization of the intracavity mean field by nonlinear quantum fluctuations was not included. Here we rectify this deficiency and fully include both static and dynamic renormalization of the pump mean field, and assess the validity and efficiency of the Green function method from a practical point of view.

The truncated Dyson equations are written in terms of two types of one-photon Green functions:

$$iD^{\zeta\zeta'}(t,t') \equiv \langle T_c(a^{\zeta\dagger}(t), a^{\zeta'}(t'))\rangle, \qquad (2.1)$$

$$\mathcal{D}^{\zeta\zeta'}(t,t') \equiv \langle T_c(a^{\zeta}(t), a^{\zeta'}(t'))\rangle, \qquad (2.2)$$

where $D^{\zeta\zeta'}, \mathcal{D}^{\zeta\zeta'}$ are the *normal* and *anomalous* propagators, respectively; and $\langle a, b\rangle = \langle ab\rangle - \langle a\rangle\langle b\rangle$. The superscripts label the different operator orderings prescribed by the Keldysh path ordering operator $T_c$ [6]. For example,

$$\begin{aligned}
iD^{++}(t,t') &= \langle T_c(a^{+\dagger}(t), a^{+}(t'))\rangle = \langle T(a^\dagger(t), a(t'))\rangle,\\
iD^{--}(t,t') &= \langle T_c(a^{-\dagger}(t), a^{-}(t'))\rangle = \langle \tilde{T}(a^\dagger(t), a(t'))\rangle,\\
iD^{-+}(t,t') &= \langle T_c(a^{-\dagger}(t), a^{+}(t'))\rangle = \langle a^\dagger(t), a(t')\rangle,\\
iD^{+-}(t,t') &= \langle T_c(a^{+\dagger}(t), a^{-}(t'))\rangle = \langle a(t'), a^\dagger(t)\rangle,
\end{aligned} \qquad (2.3)$$

and similarily for $\mathcal{D}^{\zeta\zeta'}$; $T$ and $\tilde{T}$ refer, respectively, to the usual Dyson time- and antitime-ordering operators. In the standard quantum optical formulation, the rotating wave approximation retains only energy conserving scattering processes in intermediate as well as initial and final states. For this reason it is useful to define the photon Green functions directly in term of the positive and negative frequency components of the electromagnetic field, or specifically for a cavity system, in terms of annihilation and creation operators for each of the cavity modes, as indicated in (2.1)–(2.2). A brief summary of the derivation of the full equations starting with the quantum Langevin equations for a Markovian damped system was reported elsewhere [7], and a more complete description will be given in a forthcoming paper. Here we instead concentrate on the practical application of the approximate bare-vertex theory and its comparison with other techniques.

The Dyson equations for the OPO below threshold in the bare vertex approximation are then written in Fourier space

$$\begin{aligned}
\underline{D}_1(\omega) &= \underline{\hat{D}}_1(\omega) + \underline{\hat{D}}_1(\omega)(-\underline{\sigma}_1(\omega))\underline{\mathcal{D}}_1(\omega)\\
&\quad + \underline{\hat{D}}_1(\omega)\underline{\Pi}_1(\omega)\underline{D}_1(\omega), \qquad (2.4)\\
\underline{\mathcal{D}}_1(\omega) &= (\underline{\hat{D}}_1(-\omega))^T(-\underline{\sigma}_1'(\omega))\underline{D}_1(\omega)\\
&\quad + (\underline{\hat{D}}_1(-\omega))^T(\underline{\Pi}_1(-\omega))^T\underline{\mathcal{D}}_1(\omega), \qquad (2.5)\\
\underline{D}_2(\omega) &= \underline{\hat{D}}_2(\omega) + \underline{\hat{D}}_2(\omega)\underline{P}_2'(\omega)\underline{\mathcal{D}}_2(\omega)\\
&\quad + \underline{\hat{D}}_2(\omega)\underline{\Pi}_2(\omega)\underline{D}_2(\omega), \qquad (2.6)\\
\underline{\mathcal{D}}_2(\omega) &= (\underline{\hat{D}}_2(-\omega))^T(\underline{\Pi}_2(-\omega))^T\underline{\mathcal{D}}_2(\omega)\\
&\quad - (\underline{\hat{D}}_2(-\omega))^T\underline{P}_2(\omega)\underline{D}_2(\omega), \qquad (2.7)
\end{aligned}$$

where $\underline{D}_1$ and $\underline{\mathcal{D}}_1$ are the subharmonic, normal, and anomalous Green function propagators, respectively, and similarly for the pump mode ($\underline{D}_2$ and $\underline{\mathcal{D}}_2$), and $\omega$ is the frequency offset from resonance in units of $\gamma_1$. The matrix structure of the Green functions is defined according to [6]

$$\underline{G}(\omega) = \begin{pmatrix} G^{++}(\omega) & G^{+-}(\omega) \\ G^{-+}(\omega) & G^{--}(\omega) \end{pmatrix}, \tag{2.8}$$

where $\underline{G} = \underline{D}_k$ or $\underline{\mathcal{D}}_k$ $(k = 1, 2)$. The inverse of the empty-cavity Green functions for the subharmonic field are given by

$$\hat{\underline{D}}_1^{-1}(\omega) = \begin{pmatrix} \omega + i & -2i \\ 0 & -\omega + i \end{pmatrix}. \tag{2.9}$$

The empty-cavity pump Green functions are obtained from (2.9) by letting $i \to i\gamma$. The nonlinear, many-photon processes are incorporated in the so-called *one-loop polarization* functions, where the *normal* polarization functions are given by

$$-i\Pi_1^{\alpha\beta}(\omega) = \frac{\alpha\beta}{2\pi n_{th}} \int_{-\infty}^{+\infty} d\omega'\, D_2^{\alpha\beta}(\omega') D_1^{\beta\alpha}(\omega' - \omega), \tag{2.10}$$

$$-i\Pi_2^{\alpha\beta}(\omega) = \frac{\alpha\beta}{4\pi n_{th}} \int_{-\infty}^{+\infty} d\omega'\, D_1^{\alpha\beta}(\omega') D_1^{\alpha\beta}(\omega - \omega'), \tag{2.11}$$

and the *anomalous* polarization functions are

$$P_1^{\alpha\beta}(\omega) = \frac{\alpha\beta}{2\pi n_{\rm th}} \int_{-\infty}^{+\infty} d\omega'\, \mathcal{D}_1^{\alpha\beta}(\omega') (\mathcal{D}_2^{\alpha\beta}(\omega - \omega'))^*, \quad \alpha \neq \beta \tag{2.12}$$

$$P_1^{\alpha\alpha}(\omega) = \frac{\alpha\alpha}{2\pi n_{th}} \int_{-\infty}^{+\infty} d\omega'\, \mathcal{D}_1^{\alpha\alpha}(\omega') \times (\mathcal{D}_2^{-\alpha-\alpha}(\omega - \omega'))^*, \tag{2.13}$$

$$P_2^{\alpha\beta}(\omega) = \frac{\alpha\beta}{4\pi n_{\rm th}} \int_{-\infty}^{+\infty} d\omega'\, \mathcal{D}_1^{\beta\alpha}(-\omega') \mathcal{D}_1^{\alpha\beta}(\omega - \omega'), \tag{2.14}$$

with

$$\underline{P}_1'(\omega) = \begin{pmatrix} P_1^{--}(\omega) & P_1^{+-}(\omega) \\ P_1^{-+}(\omega) & P_1^{++}(\omega) \end{pmatrix}^*, \tag{2.15}$$

and similarily for $\underline{P}_2'(\omega)$. The $\sigma$ functions represent the renormalized pump amplitude. This renormalization includes a static contribution from the anomalous propagator and a dynamical contribution from the anomalous polarization ($\sigma_z$ is the third Pauli matrix):

$$\underline{\sigma}_1(\omega) = \bar{p}^*\, \underline{\sigma}_z - \underline{P}_1(\omega), \tag{2.16}$$

$$\underline{\sigma}_1'(\omega) = \bar{p}\, \underline{\sigma}_z + \underline{P}_1'(\omega), \tag{2.17}$$

$$\bar{p} = p + \frac{\langle a_2 \rangle}{\sqrt{n_{\rm th}}} = p - \frac{1}{2\gamma n_{\rm th}} \int_{-\infty}^{+\infty} \frac{d\omega}{2\pi}\, \mathcal{D}_1^{\alpha\beta}(\omega), \tag{2.18}$$

for any $\alpha \neq \beta$, where $p$ is the pump parameter proportional to the classical intracavity pump amplitude defined in the Introduction. The corresponding diagrams are given in Fig. 1. Hence, there is a one-to-one correspondence between the elements of the diagrams and the Dyson equations, (2.4)–(2.7). Note that $\langle a_2 \rangle$ in Eq. (2.18) represents the quantum correction to the classical pump amplitude $\sqrt{n_{\rm th}} p$ (i.e., we employ the vacuum picture transformation as in Ref. [6]).

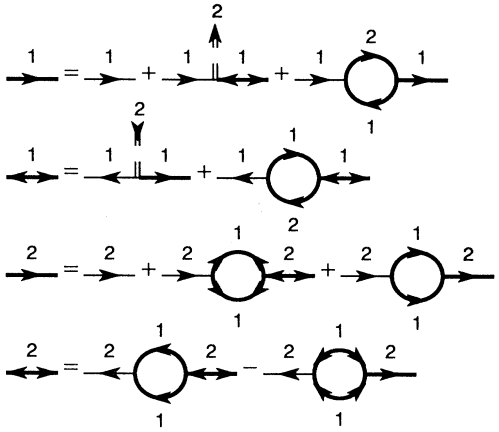

FIG. 1. Diagrammatic representation of the Dyson equations. The meaning of the parts can be read off directly from (2.4)–(2.7).

Mathematically, the Dyson equations are a coupled set of nonlinear integral equations requiring a self-consistent solution. We implement the following self-consistent iteration scheme numerically: (1) start with analytical Green functions obtained in the linearized theory [6] and evaluate the normal and/or anomalous polarization functions, at the same time renormalizing the pump field according to (2.18); (2) substitute these into the right hand side of Dyson's equations to obtain updated Green functions; (3) repeat to convergence. The converged Green functions physically account for the photon dynamics taking into account repeated resonant scattering between subharmonic photons and the classical mean pump field to all orders, as well as a class of resonant one-loop polarization processes represented by the *bubble* diagrams in Fig. 1 in which the pump field plays a dynamical role as a quantized field. These nonlinear processes introduce into the dynamics a dependence on system size, $n_{\rm th}$. It is important to appreciate that the condition for the convergence of the iteration scheme in this bare vertex approximation is distinct from the accuracy of the approximation itself, which is determined by the size of the terms omitted, i.e., higher order many-photon polarization functions generated by vertex corrections. This is discussed in detail in Sec. IV.

### B. Field observables

The observables we wish to compute are the quadrature fluctuation spectrum, intracavity photon numbers, and the pump amplitude. The spectrum of output quadrature fluctuations of the subharmonic with respect to unit shot noise is given by

$$V(X_{1\pm}, \omega) = \int_{-\infty}^{+\infty} d\tau\, e^{i\omega\tau} \langle X_{1\pm}(t+\tau), X_{1\pm}(t) \rangle = 1 + 4\{iD_1^{-+}(\omega) \pm \mathrm{Re}[\mathcal{D}_1^{++}(\omega)]\} \tag{2.19}$$

where $X_{1+} = a_{1,out} + a_{1,out}^\dagger$ and $X_{1-} = (a_{1,out} - a_{1,out}^\dagger)/i$

are the output amplitude and phase quadrature operators. The boundary condition at the output mirror has been properly accounted for by using the relation $a_{1,out}(t) - a_{1,in}(t) = \sqrt{2}a_1(t)$, to express (2.19) in terms of internal field operators [15]. Thus the Green functions, which are defined in terms of internal field operators, determine the spectrum directly. The intracavity subharmonic and pump photon numbers are given by

$$\langle n_k \rangle = \langle (a_k^\dagger + \alpha_k^*)(a_k + \alpha_k) \rangle = \int_{-\infty}^{+\infty} d\omega \, iD_k^{-+}(\omega) + |\alpha_k + \langle a_k \rangle|^2, \qquad (2.20)$$

where $k$ =1,2 and $\alpha_k$ is the classical field amplitude [8]. The quantum correction $\langle a_2 \rangle$ to the pump amplitude $p$ can be deduced from (2.18).

## III. ANALYTICAL RESULTS: THE ONE-POLE APPROXIMATION

Following Refs. [6] and [16], Plimak and Walls [13] have derived an analytical result for the quadrature fluctuations in an OPO below threshold. In this section we derive these results from the bare-vertex equations, and illustrate the underlying physics diagrammatically. In addition, this discussion serves to motivate the numerical comparisons discussed in Sec. V. The analysis is based upon the important observation that under certain approximations the below threshold nonlinear theory has a similar structure to the linearized theory above threshold, $p > 1$. In particular, by comparing the diagrammatic structure of Figs. 2 and 3, one sees that the nonlinear subharmonic fluctuations below threshold, described by the one-loop polarization function, play a dynamical role analogous to the subharmonic mean field above threshold. As a result, one can identify an effective subharmonic mean field with the subharmonic quantum fluctuations. This indicates how the subharmonic mean field, which condenses at threshold in the classical theory, arises from the growth of quantum fluctuations below the classical threshold, consistent with the view that quantum fluctuations smooth out the classical threshold.

Figure 2 shows the diagrams when only pump dissipation is retained in the pump dynamics, i.e., the pump propagators are approximated by the empty-cavity propagators. The linearized above threshold theory of the OPO is shown for comparison in Fig. 3, where scattering from the classical pump and subharmonic mean fields takes place. The self-energy contribution in Fig. 3 may be written down by inspection as $s^2\alpha\beta\hat{D}_2^{\alpha\beta}(\omega)$, where $s^2$ ($s^2 \equiv |\alpha_1|^2/n_{\rm th}$) comes from the two mean-field lines [6]. The corresponding polarization integral in Fig. 2, and defined in (2.10), may be written in an analogous form as

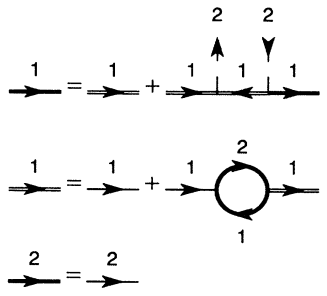


FIG. 2. Diagrammatic representation of the Dyson equations in the adiabatic limit. The pump Green functions are replaced by empty-cavity Green functions, i.e. only Markovian dissipation is retained. The vertical, dashed lines retain only static renormalization of the pump amplitude, $\underline{\sigma}_1(\omega), \underline{\sigma}_1'(\omega) \to \bar{p}\underline{\sigma}_z$ in (2.16) and (2.17).

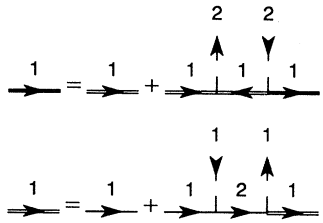


FIG. 3. Diagrammatic representation of linearized above-threshold Dyson equations. The subharmonic mean field, $s$, is represented by a vertical dashed line labeled 1.

$$\Pi_1^{\alpha\beta}(\omega) = \frac{i\alpha\beta}{2\pi\, n_{\rm th}} \int_{-\infty}^{+\infty} d\omega' \, D_2^{\alpha\beta}(\omega') D_1^{\beta\alpha}(\omega' - \omega) \approx \alpha\beta\hat{D}_2^{\alpha\beta}(\omega) \int_{-\infty}^{+\infty} d\omega' \left(\frac{i}{2\pi\, n_{\rm th}}\right) D_1^{\beta\alpha}(\omega') \approx \alpha\beta\hat{D}_2^{\alpha\beta}(\omega) \left[\frac{p}{4n_{\rm th}(1-p)}\right] \qquad (3.1)$$

under the approximations that (i) the Green functions in (3.1) are given by linearized below threshold Green functions, (ii) only the dominant pole $\omega = \pm i(1-p)$ is retained, and (iii) $\gamma \gg (1-p)$. Thus in agreement with Ref. [13], we may identify an effective subharmonic mean field squared as

$$s^2 = \frac{p}{4n_{\rm th}(1-p)}. \qquad (3.2)$$

In addition, we may compute the renormalized pump amplitude (2.18)

$$\bar{p} = p - \frac{p}{8n_{\rm th}\gamma(1-p)}. \qquad (3.3)$$

The last results, (3.2) and (3.3), may be improved upon in the following way. One solves for the Green functions of Fig. 2 with $\Pi_1$ given in (3.1). Note that the pump Green functions remain equal to the empty-cavity functions which physically accounts only for Markovian dissipation. Then derive a new expression for $\Pi_1$ by using the updated subharmonic Green functions to get

$$s_{new}^2 = \frac{\bar{p}}{4n_{\rm th}(1-\bar{p}+s^2/\gamma)}. \qquad (3.4)$$

The new renormalized pump amplitude follows by using the updated Green functions in (2.18):

$$\bar{p}_{new} = p - \frac{\bar{p}}{8n_{\rm th}\gamma\,(1-\bar{p}+s^2/\gamma)}. \qquad (3.5)$$

Similarily, this requires (i) taking the dominant pole $\omega = \pm i(1-\bar{p}+s^2/\gamma)$, and (ii) assuming $\gamma \gg (1-\bar{p}+s^2/\gamma)$. If this procedure is repeated then we arrive at the iteration scheme defined by the algebraic equations

$$s^2 = \frac{\bar{p}}{4n_{\rm th}(1-\bar{p}+s^2/\gamma)}, \tag{3.6}$$

$$\bar{p} = p - \frac{\bar{p}}{8n_{\rm th}\gamma\,(1-\bar{p}+s^2/\gamma)}. \tag{3.7}$$

Once converged values for $s^2$ and $\bar{p}$ are found, the observables may then be obtained by substituting these into well known expressions for the linearized above threshold theory [12]. Thus

$$V(X_{1\pm},\omega) = 1 \pm \frac{4\bar{p}(\omega^2+\gamma^2)}{[\gamma(1\mp\bar{p})+s^2-\omega^2]^2+\omega^2(1+\gamma\pm\bar{p})^2}, \tag{3.8}$$

$$\langle n_1\rangle = \int_{-\infty}^{+\infty} d\omega\, iD_1^{-+}(\omega), \tag{3.9}$$

where

$$iD_1^{-+}(\omega) = \frac{\bar{p}}{2}(\omega^2+\gamma^2)\left\{\frac{1}{[\gamma(1-\bar{p})+s^2-\omega^2]^2+\omega^2(1+\gamma-\bar{p})^2} - \frac{1}{[\gamma(1+\bar{p})+s^2-\omega^2]^2+\omega^2(1+\gamma+\bar{p})^2}\right\}. \tag{3.10}$$

A very practical feature of this result is that it involves only iteration of algebraic equations rather than integral equations. The theory clearly shows how nonlinear quantum noise behaves dynamically like a mean field, which influences the subharmonic fluctuations below the classical threshold in the same way that the subharmonic mean field does in the linearized above threshold OPO.

The analytic results for subharmonic fluctuations ignore the pump dynamics except for Markovian dissipation. In a regime where both the analytic solution and the bare vertex theory are valid, differences in computed quantities are due to the influence of nonlinear pump fluctuations on the subharmonic dynamics. This is illustrated in Sec. V.

## IV. BARE-VERTEX THEORY: EXPANSION PARAMETER AND VALIDITY

In this section we explore the limitations of the bare-vertex OPO theory leading to the Dyson equations (2.4)–(2.7). There are two main issues to address: (1) the range of *validity* of the bare-vertex approximation, and (2) the *convergence* of the bare-vertex solutions (recall that the Dyson equations are solved numerically by iterating the integral equations [6]). These issues are distinct, and we will find that the solutions can converge outside of the range of validity of the bare-vertex approximation.

With regard to the bare-vertex approximation, recall that the closed form Dyson equations are obtained by truncating the vertex part at zeroth order in the threshold pump photon number $n_{\rm th}$ [6]. However this procedure, like the linearization procedure, is not uniformly valid in the pump parameter $p$, or equivalently, the distance to threshold $1-p$. We expect that complex photon correlations arising from higher order photon polarization processes will become increasingly important near to oscillation threshold. The validity of the method will depend not only on $n_{\rm th}$ and $1-p$, but the other system parameter $\gamma$ as well as frequency $\omega$.

The radius of convergence is likewise determined by $n_{\rm th}$, $1-p$, and $\gamma$. The proper framework for its estimation is multiplicative renormalization group theory (RGT), which takes advantage of the invariance of Dyson's equations to multiplicative transformations. We will not discuss this further here, but instead give an argument which leads to the same result for the radius of convergence.

### A. Radius of convergence of bare-vertex equations

As discussed in Ref. [6], Fig. 2 is an equivalent representation of the subharmonic propagators of Fig. 1 when the polarization functions are evaluated using linearized Green functions (see Sec. III). In this representation, the nonlinear theory is obtained by renormalizing the empty-cavity Green functions of the linearized theory. To obtain the conditions for convergence near threshold ($p=1$), it is sufficient to consider the renormalized empty-cavity Green function at zero frequency detuning, which we denote as $\underline{\tilde{D}}_1(0)$. Furthermore, we will consider the $\tilde{D}_1^{++}(0)$ matrix element of $\underline{\tilde{D}}_1(0)$. This is a reasonable reduction since we expect the matrix elements of $\underline{\tilde{D}}_1(0)$ to have the same scaling behavior near threshold. The Dyson equation is given by

$$\tilde{D}_1^{++}(0) = \hat{D}_1^{++}(0) + \hat{D}_1^{++}(0)\Pi_1^{++}(0)\tilde{D}_1^{++}(0), \tag{4.1}$$

where

$$\Pi_1^{++}(0) \approx \frac{-ip}{4n_{\rm th}\gamma(1-p)}, \tag{4.2}$$

near threshold. The solution can be obtained algebraically, and is given by

$$\tilde{D}_1^{++}(0) = \frac{\hat{D}_1^{++}(0)}{1-\hat{D}_1^{++}(0)\Pi_1^{++}(0)} = \hat{D}_1^{++}(0)\sum_{n=0}^{\infty}(\hat{D}_1^{++}(0)\Pi_1^{++}(0))^n. \tag{4.3}$$

Thus the Green function will converge absolutely if

$$g \equiv |\hat{D}_1^{++}(0)\Pi_1^{++}(0)| = \frac{1}{4n_{\rm th}\gamma(1-p)} < 1, \qquad (4.4)$$

where we have identified the absolute value of the term in parentheses in (4.3) as the effective expansion parameter of the bare-vertex theory. The algebraic structure of the system-size expansion parameter is what we expect, intuitively. We expect that the strength of the system-size parameter should scale inversely with the distance from threshold, the pump threshold photon number and the cavity lifetime. Equation (4.4) is supported by RGT methods, where $g$ is known as the invariant coupling constant.

We have obtained an approximate expression for the radius of convergence, which predicts that an iterative solution will not converge sufficiently close to threshold. Apparently we also have a criterion for the validity of the theory expressed as a condition on the distance from threshold, $(1-p) > 1/4n_{\rm th}\gamma$ from (4.4). This would be true if the size of the polarization processes left out of the bare-vertex theory remained small compared to the one-loop polarization processes retained in the theory. The latter does not hold as we get closer to the classical threshold point $p = 1$. We show in the following section that the leading polarization corrections become important before the bare-vertex convergence breaks down. Therefore, we arrive at a stricter validity criterion by requiring that the leading polarization corrections remain small compared to the one-loop polarization functions.

### B. Validity: estimate of vertex corrections

In the bare-vertex approximation, the vertex part is approximated by unity, giving the polarization functions, (2.10)–(2.15), a simple *bubble* topology, as illustrated in Fig. 1. We arrive at a validity citerion by requiring that the leading polarization corrections remain small in comparison with the bare-vertex, or simple *bubble* type, polarization functions. As a specific example, consider the leading $\underline{\pi}_1$ polarization correction in Fig. 4 that is generated by the corresponding vertex correction in Fig. 5. Using the diagrams in Fig. 1, it is easy to see, by energy conservation at the vertices, that the leading corrections to the other polarization functions ($\underline{\pi}_2$, $\underline{P}_2$, and $\underline{P}_2'$) will also be generated by a vertex correction consisting of two anomalous subharmonic Green functions and one anomalous pump Green function. Therefore, $\underline{\pi}_1$ typifies the general behavior in regard to leading vertex corrections.

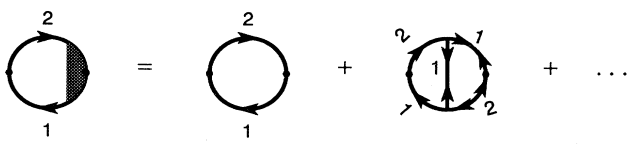


FIG. 4. Diagrammatic representation of the expansion of the photon polarization, (4.6) and (4.8). The first term on the right corresponds to the bare-vertex approximation, and the second term is the leading correction given in (4.8).

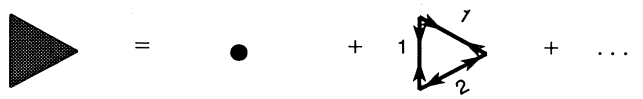


FIG. 5. Diagrammatic representation of the expansion of the vertex part (4.7). The triangle emphasizes that the vertex part has three external vertices (see Fig. 4). The first term on the right hand side is the bare vertex, represented by a point, and the second term is the leading correction (4.9).

Furthermore, we will focus on one matrix element of $\underline{\pi}_1$, namely $\pi_1^{++}$. This is a reasonable reduction since we expect the matrix elements of $\underline{\pi}_1$ to have the same scaling behavior near threshold ($p = 1$), where vertex correction become important.

The exact functional form for the $\pi_1^{++}$ polarization function follows from the full matrix Dyson equations [7] and is given by

$$-i\pi_1^{++}(\omega) = \frac{1}{2\pi\, n_{\rm th}} \sum_{\zeta_1,\zeta_2} \int_{-\infty}^{+\infty} d\omega'\, D_1^{+\zeta_1}(-\omega') \times \Gamma^{\zeta_1+\zeta_2}(-\omega',\omega) D_2^{\zeta_2+}(\omega-\omega'), \qquad (4.5)$$

where $D_1^{++}$ and $D_2^{++}$ are exact Green functions matrix elements and $\Gamma^{\zeta_1+\zeta_2}$ are exact vertex elements. There are four terms that contribute to $\pi_1^{++}$ since $\zeta_1, \zeta_2 = +$ or $-$. Assuming that all four vertex functions in (4.5) have the same scaling behavior near threshold, the largest value attainable in (4.5) is if all vertex functions add up coherently, and we evaluate $\pi_1^{++}$ at $\omega = 0$. Therefore, to consider the worst case scenario, we calculate one vertex element explicitly and multiply by a factor of 4; for example we take $\Gamma^{\zeta_1+\zeta_2} \to 4\Gamma^{+++}$. Consequently, the polarization and vertex functions to leading corrections, corresponding to Figs. 4 and 5, respectively, are given by

$$\pi_1^{++}(0) \approx \Pi_1^{++}(0) + \delta\Pi_1^{++}(0), \qquad (4.6)$$

$$\Gamma^{+++}(-\omega,0) \approx 1 + \delta\Gamma^{+++}(-\omega,0), \qquad (4.7)$$

where

$$\delta\,\Pi_1^{++}(0) \approx \frac{i}{2\pi\, n_{\rm th}} \int_{-\infty}^{+\infty} d\omega' D_1^{++}(-\omega') \times 4\delta\Gamma^{+++}(-\omega',0) D_2^{++}(-\omega') \qquad (4.8)$$

$$\delta\Gamma^{+++}(-\omega,0) = \frac{1}{2\pi\, n_{\rm th}} \int_{-\infty}^{+\infty} d\omega' \times (\mathcal{D}_1^{--}(\omega'+\omega)\mathcal{D}_1^{--}(\omega'))^* \mathcal{D}_2^{++}(\omega'), \qquad (4.9)$$

and $\Pi_1^{++}(0)$ is given in (4.2). The bare-vertex polarization function in (4.2) was approximated using linearized Green functions. Likewise, we will use linearized Green functions to compute $\delta\Pi_1^{++}$, but first we must estimate the vertex correction $\delta\Gamma^{+++}$.

The Green functions that enter into the vertex equation, (4.9), are obvious from the diagrams in Fig. 5 (the explicit functional form is given in a forthcoming paper). Note from the diagrams in Fig. 1 that there is no linearized contribution to $\underline{\mathcal{D}}_2$, i.e., the pump field is in a co-

herent state in the linearized approximation. Therefore, to obtain an analytical expression for $\mathcal{D}_2^{++}$, we approximate the anomalous pump Green function matrix (2.7) by

$$\underline{\mathcal{D}}_2(\omega) \approx -(\underline{\hat{D}}_2(-\omega))^T \underline{P}_2(\omega)\underline{\hat{D}}_2(\omega). \tag{4.10}$$

The integral in (4.9) is approximated by its dominant terms arising from poles at $-\omega \pm i(1-p)$, $\pm i(1-p)$, and $\pm 2i(1-p)$, and the result is

$$\delta\Gamma^{+++}(-\omega,0) \approx \frac{5p^2}{384 n_{\rm th}^2 \gamma^2 (1-p)^4}\,\mathcal{D}_1^{--}(-\omega). \tag{4.11}$$

When the vertex correction (4.11) is substituted into (4.8), the polarization correction reduces to

$$\delta\Pi_1^{++}(0) \approx \left(\frac{1}{2\pi i}\right)\left(\frac{-5p}{3\times 2^7 n_{\rm th}^3\gamma^2(1-p)^4}\right) \times \int_{-\infty}^{+\infty} \frac{(\omega'+i)d\omega'}{(\omega'-i\gamma)[\omega'^2+(1-p)^2]^2}. \tag{4.12}$$

The integral is approximated by its dominate term arising from the second order pole at $\pm i(1-p)$. Consequently, we arive at the following expression:

$$\delta\Pi_1^{++}(0) \approx \frac{5ip}{3\times 2^9 n_{\rm th}^3\gamma^3(1-p)^6}[1+\gamma^{-1}-(1-p)^{-1}]. \tag{4.13}$$

Consider the case where $(1-p) \ll 1, \gamma$. From (4.13) we have

$$\delta\Pi_1^{++}(0) \approx \frac{-5ip}{3\times 2^9 n_{\rm th}^3\gamma^3(1-p)^7}. \tag{4.14}$$

We take (4.14) to be our final approximation to the polarization correction. Only in severe nonadiabatic conditions will (4.14) not follow from (4.13), and $\delta\Pi_1^{++}(0)$ will not simply scale as a product of $n_{\rm th}\gamma$.

Recall that validity of the bare-vertex approximation hinges on the requirement that the next higher order corrections to the polarization functions remain small compared to the simple bubble (bare-vertex) polarization functions. Thus from the above analysis the validity criterion is established through

$$\frac{\|\delta\Pi_1^{++}(0)\|}{\|\Pi_1^{++}(0)\|} \ll 1. \tag{4.15}$$

Substituting (4.2) and (4.14) into (4.15), the validity criterion for the bare-vertex approximation takes the form of a restriction on the distance from threshold:

$$(1-p) \gg 0.48\left(\frac{1}{n_{\rm th}\gamma}\right)^{\frac{1}{3}}. \tag{4.16}$$

The validity of the bare-vertex approximation has been determined semiquantitatively. The diagrams in Fig. 1 correctly describe the quantum dynamics of the OPO system when (4.16) is satisfied. When the criterion is violated, other photon scattering processes of the type indicated in Fig. 4 become equally important, if not more so, in accurately describing the dynamics of the system. In practice, however, we find that the bare-vertex solutions are accurate even when the distance from threshold equals the RHS of (4.16). This is illustrated in Sec. V.

## V. RESULTS

Here we discuss the influence of nonlinear quantum noise on intracavity field amplitude and photon number, and output quadrature squeezing spectra for the OPO. We further compare the accuracy and efficiency of Green function computations with results generated from the analytical complex $P$ distribution (see the Appendix), the one-pole approximation [13] of Sec. III, and the wavefunction simulation method (see the Appendix). The analytical complex $P$ method is restricted to evaluating moments in the adiabatic regime, $\gamma \gg 1$. Although one can obtain spectral quantities from the positive $P$ distribution via stochastic simulations, the reliability of this method in the nonlinear regime has been questioned [5] and we have not investigated its use here. In the nonadiabatic regime, we compare the Green function solutions with the one-pole approximation and the wavefunction simulation method. The wavefunction simulation method can, in principle, also calculate spectral quantities. However, the numerical computations are extremely time consuming and it is difficult to independently assess the accuracy of the results. On the other hand, the mean values and the spectral quantities are obtained simultaneously, on the order of CPU seconds, in the Green function method.

In Fig. 6 the bare-vertex solution to the intracavity subharmonic photon number is shown for various pump values versus the iteration number, in the adiabatic limit $\gamma = 100$ and $n_{\rm th} = 10$. The iteration number indicates the number of steps through the self-consistent iteration scheme outlined in Secs. II A and III. These results are compared with the complex $P$ distribution and the one-pole approximation. For this parameter set, $n_{\rm th}\gamma = 10^3$, the validity criterion derived by Plimak and Walls [13] specifies that $p \ll 0.97$. Our validity criterion, (4.16), based on vertex estimates, specify that $p \ll 0.95$. Equation (4.16) appears to overestimate the error in the sense that the bare-vertex equations are accurate all the way up to the boundary of the criterion $p = 0.95$. Even beyond the range of validity, the bare-vertex equations are in better agreement with the complex $P$ results than the one-pole approximation. The comparison in Fig. 6 between the bare-vertex theory and the one-pole approximation illustrates the quantitative influence of nonlinear pump fluctuations, which we retain in the bare-vertex theory, on the subharmonic photon number. In Fig. 6(d), where $p = 0.99$, we illustrate the breakdown of convergence of the iterative solution of the Dyson equations. The criterion of Sec. IV A predicts convergence of the bare-vertex solutions is to be expected for $p < 0.9998$. Similar to the validity criterion, convergence is found up to the boundary of (4.4). It is interesting to note that the many-body theory appears to converge to the correct solution before

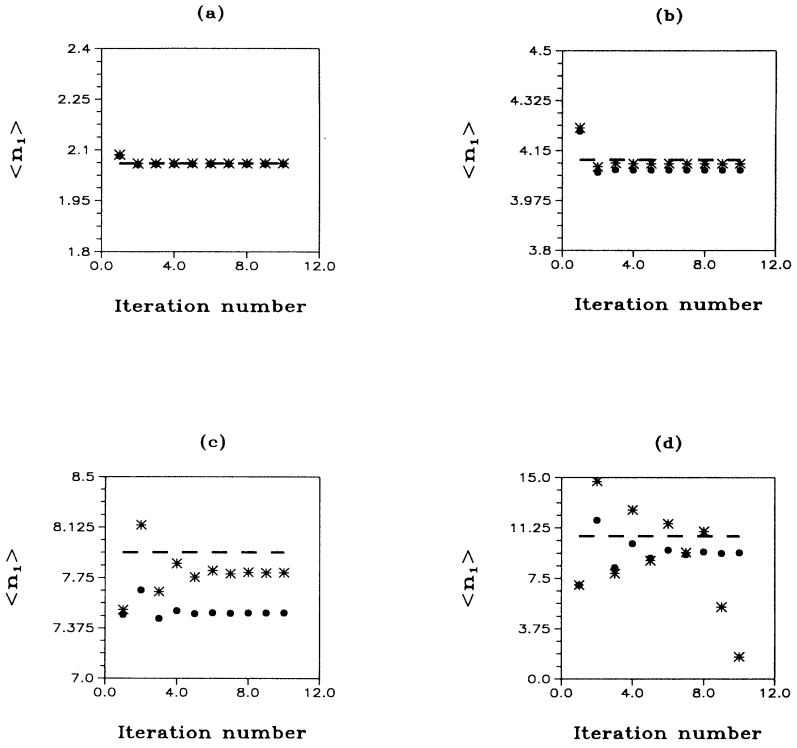


FIG. 6. Comparison of subharmonic photon number versus iteration number for the adiabatic complex $P$ method (dashed line), the one-pole approximation (3.9) and (3.10) (solid circles) and the Green function method (asterisk). Parameters are $n_{\rm th} = 10$ and $\gamma = 100$ for (a) $p = 0.90$, (b) $p = 0.95$, (c) $p = 0.98$, and (d) $p = 0.99$.

it breaks down, reminiscent of an asymptotic expansion.

In Fig. 7 we show the squeezing spectrum for a range of pump values from $p = 0.90$ to $p = 0.98$. The values for $n_{\rm th}$ and $\gamma$ are the same as those in Fig. 6. The one-pole approximation agrees quantitatively with the bare-vertex equations up to about $p = 0.95$, the boundary of the validity criterion.

In Fig. 8 the bare-vertex solution to the intracavity subharmonic photon number is shown for various pump values versus the iteration number, in the nonadiabatic limit where $\gamma = 0.1$ and $n_{\rm th} = 10^3$. These results are compared with the wave-function simulation method and the one-pole approximation. The one-pole approximation is not expected to be valid under these nonadiabatic conditions, since $\gamma \sim (1 - \bar{p} + s^2/\gamma)$; however, we find that it is quite accurate for the chosen parameter set of Fig. 8. For $p = 0.80, 0.85, 0.90$ the simulation results are calculated to a precision of $\pm 0.01$; for $p = 0.93$, the result is accurate to $\pm 0.1$. For this parameter set, $n_{\rm th}\gamma = 100$, the validity criterion (4.16) specifies that $p \ll 0.90$. Similar to the adiabatic regime, we observe that the bare-vertex solutions are valid up to the boundary of the criterion (4.16). The computation time for the bare-vertex equations, which include calculation of dynamic spectra and stationary mean values for a given parameter set, is of the order of CPU seconds on a modest workstation. However, the stationary or equal time averages computed using a parallelized wave-function simulation method, which ran on 32 processors simultaneously, requires a computation time on the order of CPU hours near threshold.

To calculate dynamic spectra with this approach requires the simulation of auxiliary functions in addition to the wave functions, according to the quantum regression theorem [9]. This is an extremely intensive numerical procedure in the application considered here. As an illustration Fig. 9 shows the squeezing spectrum as calculated for $p = 0.5$, $n_{\rm th} = 100$, and $\gamma = 1$, and compared to our bare-vertex results. In an effort to reduce the computational expense we followed the method of Mølmer and Dalibard and averaged one (as opposed to several) set of auxiliary functions per wave function. This approach worked successfully in a test run of the analytically known linearized squeezing spectrum. The simulation in Fig. 9 which used parallelized computer code was run on a KSR2-64 using 32 processors simultaneously and took hundreds of CPU hours, averaging 49 000

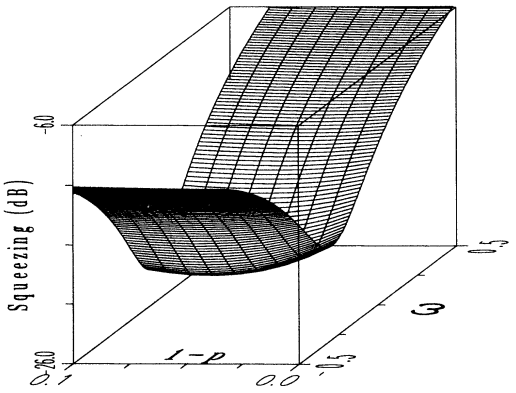


FIG. 7. Spectrum of squeezing versus distance from threshold $(1-p)$ and frequency $\omega$ for $n_{\rm th} = 10$ and $\gamma = 100$. Squeezing is given by $V(X_{1-}, \omega)$ in (2.19).

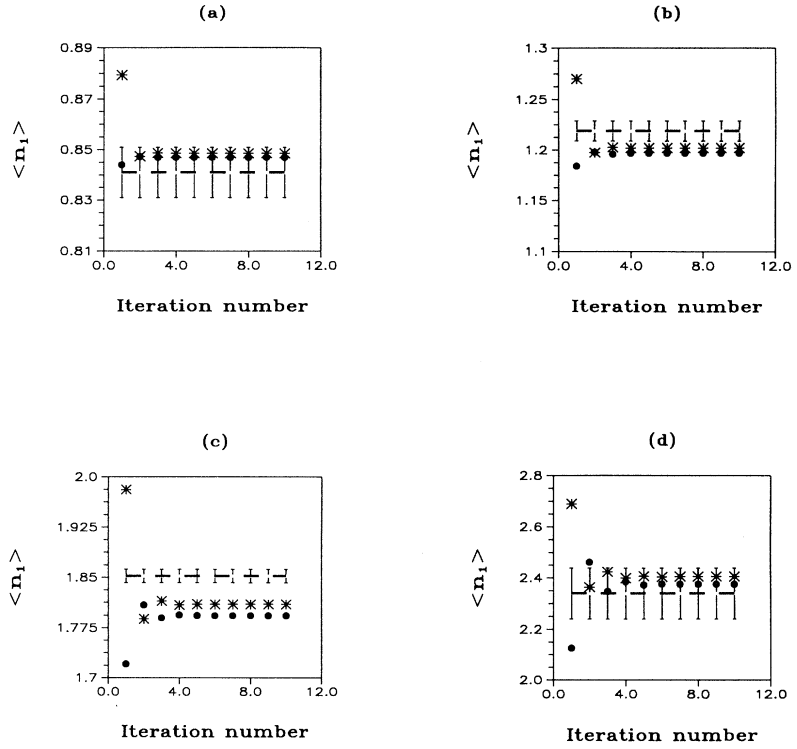


FIG. 8. Comparison of subharmonic intracavity photon number versus iteration number for the wave-function simulation method (dashed line with error bars), the one-pole approximation (3.9) and (3.10) (solid circles), and the Green function method (asterisk). Parameters are $n_{\rm th} = 1000$ and $\gamma = 0.1$ for (a) $p = 0.80$, (b) $p = 0.85$, (c) $p = 0.90$, and (d) $p = 0.93$.

wave functions. The result is disappointing, and is not yet fully converged. The simulations have converged to the bare-vertex solution at low frequencies but not at higher frequencies. We do observe a slow trend towards the bare-vertex solution at higher frequencies as more trajectories are averaged. It is likely that faster convergence would be obtained by averaging sets of $N$ auxiliary functions per wave function, but still at an enormous expense compared to the bare-vertex method. We should also note that with critical slowing down the simulation method would be even more expensive in the region near threshold where the bare-vertex method breaks down, so it does not appear to present a practical alternative until a significantly more efficient computational procedure is found.

In Figs. 10 and 11 the bare-vertex solution for the pump photon number and the quantum correction to the classical pump amplitude $\langle a_2 \rangle$ are given, respectively, versus iteration number for various pump values. The pump observables are not accessible to the one-pole approximation, and so, we compare with wave-function simulations in the nonadiabatic regime where $n_{\rm th} = 10^3$ and $\gamma = 0.1$. By contrast with the subharmonic, the accuracy of these pump observables is not restricted by (4.16). This can be explained by the qualitatively different dynamics of the pump and subharmonic near threshold. The latter undergoes a "condensation" and is much more sensitive to fluctuations.

In Fig. 12 we show the squeezing spectrum versus cavity detuning for a range of pump values from $p = 0.90$ to $p = 0.96$. The values for $n_{\rm th}$ and $\gamma$ are the same as those in Figs. 8–11. Notice the qualitatively nonlinear feature in the spectrum, the positive peak centered at $\omega = 0$. This peak begins to emerge at $p = 0.91$, where the accuracy of the bare-vertex solutions begins to break down. Higher pump values enhance this feature as indicated in Fig. 12, and we expect the figure to qualitatively represent the true spectrum. The one-pole approximation also gives a qualitatively similar spectrum for this parameter set. Quantitative analysis of the growth of this feature as the classical threshold is approached would require fully

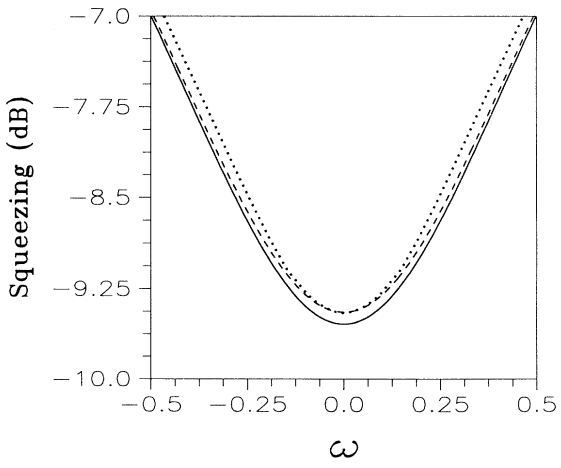


FIG. 9. Comparison of the squeezing spectrum versus frequency $\omega$ for the wave-function simulation method (dotted line) and the Green function method (dashed line). The linearized spectrum (solid line) is shown for comparison. Parameters are $n_{\rm th} = 100$, $\gamma = 1$, and $p = 0.5$. Squeezing is given by $V(X_{1-}, \omega)$ in (2.19).

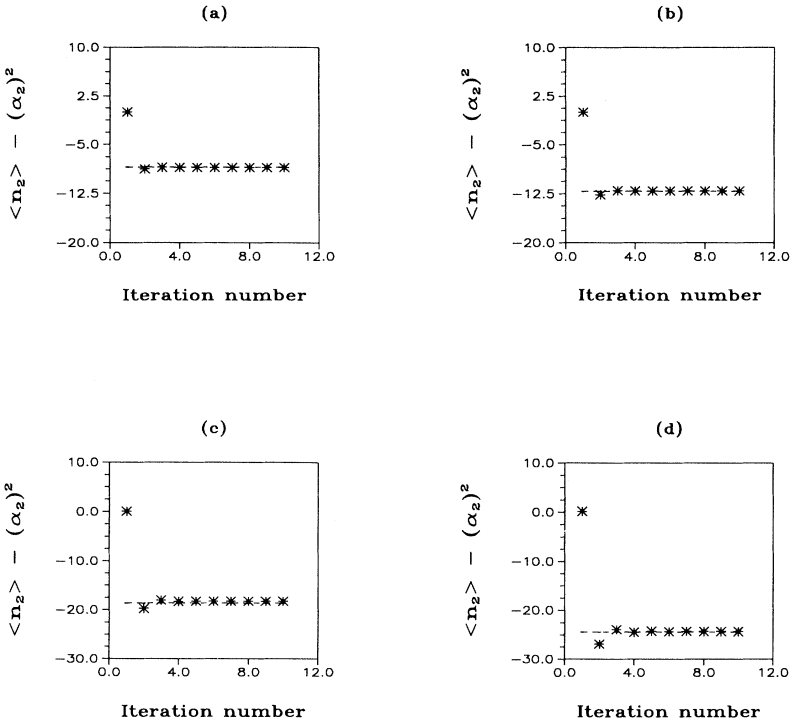


FIG. 10. Comparison of pump intracavity photon number (relative to the classical photon number $\alpha_2^2$) versus iteration number for the wave-function simulation method (dashed line) and the Green function method (asterisk). Error bars for the latter are not visible on this scale. Parameters are $n_{\rm th} = 1000$ and $\gamma = 0.1$ for (a) $p = 0.80$, (b) $p = 0.85$, (c) $p = 0.90$, and (d) $p = 0.93$.

nonperturbative methods, more powerful than those discussed here.

## VI. CONCLUSION

The quantum statistical properties of dissipative quantum optical systems measurable by photodetection can be expressed in terms of photon Green functions. In this paper we have investigated the application of a method which calculates such Green functions directly, to study the influence of nonlinear quantum fluctuations near the threshold of a degenerate OPO. New results on stationary intracavity field amplitude and photon number, and output squeezing spectra have been computed in this way,

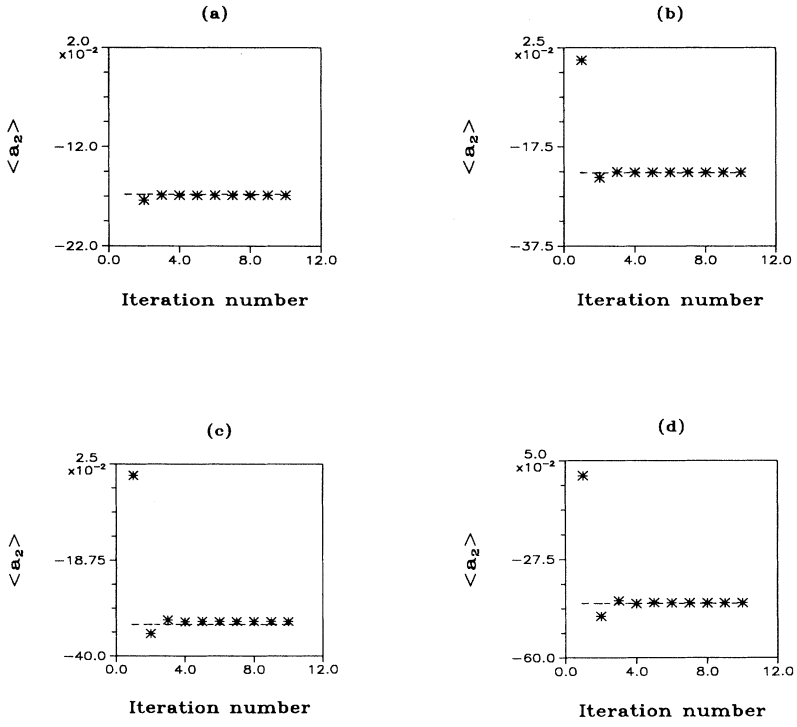


FIG. 11. Comparison of quantum corrections to the classical pump amplitude $\langle a_2 \rangle$ versus iteration number for the wave-function simulation method (dashed line with error bars) and the Green function method (asterisk). Parameters are $n_{\rm th} = 1000$ and $\gamma = 0.1$ for (a) $p = 0.80$, (b) $p = 0.85$, (c) $p = 0.90$, and (d) $p = 0.93$.

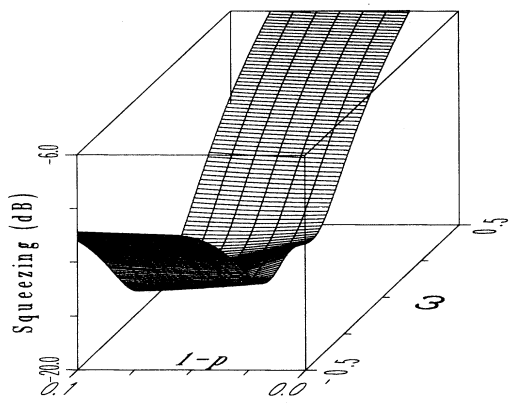


FIG. 12. Spectrum of squeezing versus distance from threshold $(1-p)$ and frequency $\omega$. Parameters are $n_{\rm th} = 1000$ and $\gamma = 0.1$. Squeezing is given by $V(X_{1-}, \omega)$ in (2.19).

using both analytic approximations and numerical methods. The reduction of squeezing at low frequencies as threshold is approached was shown, consistent with the results of Refs. [6] and [13], to be due to nonlinear photon polarization (represented by a *bubble* diagram) which mimics a finite electric-field amplitude, even when the latter is zero.

With any theoretical method, a careful assessment of its validity and how it compares with other approaches is important. For this reason we have presented a detailed discussion of the range of validity and convergence properties of the bare-vertex approximation employed to truncate the hierarchy. The criteria derived are in agreement with the numerical results presented. Analytical approximations to the photon Green functions capture the qualitative features of the bare-vertex truncation, and only quantitative differences due to nonlinear quantum fluctuations of the pump are observed. An exact numerical treatment of quantum correlations in the degenerate OPO is formidable by any method based on Fock space expansions, except at very low photon numbers, because one must deal with two quantized field modes and very large basis sets. We have used the complex $P$ distribution, the wave-function simulation method and analytic approximations to confirm the accuracy of the Green function method for the calculation of stationary states and quantum correlation functions. We find that the calculation of single time averages alone using wave-function simulations is more computationally intensive than the calculation of both stationary states and stationary dynamic spectra using photon Green functions. Moreover, two-time correlations and spectra require extensive auxiliary calculations with the wavefunction simulation method which makes it impractical by comparison. Spectral simulations of stochastic differential equations derived from the positive $P$ distribution are more competitive as they are based on coherent state rather than number state expansions, but are not considered here [17]. Density matrix methods are exact in principle, but near threshold would require both sparse storage and supercomputing facilities. The reason the Green function approach fairs so well by comparison is because extraneous information retained in both density matrix and wave-function simulation methods is discarded.

The nonlinear quantum fluctuations in the vicinity of the OPO threshold are characteristic of the underlying classical pitchfork bifurcation. By contrast in intracavity second harmonic generation there is a Hopf bifurcation, where the signature of nonlinear quantum fluctuations is quite different. This will be reported in a forthcoming paper along with results on the behavior of the OPO above the classical threshold and a complete derivation of the equations for the photon Green functions, including those employed here.

## ACKNOWLEDGMENTS

This research was supported by NSF Grant No. PHY-9413504 and a NATO international travel award. The work of D.N. and H.H.R. (in part) was supported by the NSF REU program. T.A.B.K. thanks F. Haake, L.I. Plimak, S. Swain, and D.F. Walls for discussions.

## APPENDIX

Below we briefly describe two independent methods that were used for comparison with the Green function solutions. Mean values for the subharmonic photon number in the adiabatic regime, $\gamma \gg 1$, are compared with analytical values obtained via the complex $P$ distribution [8]. In the nonadiabatic regime, mean values for the pump field and intracavity photon numbers, and output squeezing spectra are compared with the wave-function simulation method [9].

### 1. Complex $P$ distribution

By expanding the density operator in terms of the complex $P$ quasiprobability distribution, the OPO master equation with the pump mode adiabatically eliminated on the basis that $\gamma \gg 1$, can be converted to a Fokker-Planck equation [8]. This satisfies potential conditions enabling the stationary probability distribution $P(\alpha_1, \alpha_1^\dagger)$ to be given explicitly. All normally ordered stationary moments of the subharmonic can then be found by quadratures over contours in two copies of the complex plane:

$$I_{nn'} \equiv \langle a_1^{\dagger n} a_1^{n'} \rangle = \int_C \int_C \alpha_1^{\dagger n} \alpha_1^{n'} P(\alpha_1, \alpha_1^\dagger) d\alpha_1^\dagger d\alpha_1. \quad \text{(A1)}$$

The contours may be deformed so that the integrals define the Gauss hypergeometric function ${}_2F_1$, hence,

$$I_{nn'} = N \sum_{m=0}^{\infty} \frac{2^m}{m!} (-c)^{m+n'} (-c^*)^{m+n} \times \{{}_2F_1[-(m+n'), j, 2j, 2]\} \times \{{}_2F_1[-(m+n), j, 2j, 2]\}, \quad \text{(A2)}$$

where

$$c \equiv \sqrt{2n_{\rm th}\gamma p} \quad \text{and} \quad j \equiv 2n_{\rm th}\gamma, \tag{A3}$$

and $N$ is the normalization constant.

### 2. Wave-function simulation method

In the nonadiabatic limit, we follow the wave-function simulation method set forth by Mølmer *et al.* [9]. In this prescription a non-Hermitian Hamiltonian generates a smooth evolution which is randomly interrupted by quantum jumps. Quantum single-time expectation values may be constructed from the wave-function evolution averaged over many trajectories. Two-time correlation functions may be calculated by a similiar procedure derived from application of the quantum regression theorem, but involving the evolution of some auxiliary quantities in addition to the wave function. The state vector is expanded in a Fock basis of size $(N_1+1)(N_2+1)$, i.e., $0 < n_1 < N_1$, $0 < n_2 < N_2$, where $N_1$ and $N_2$ are large enough to neglect boundary effects,

$$|\Psi(t)\rangle = \sum_{n_1=0}^{N_1}\sum_{n_2=0}^{N_2} b_{n_1,n_2}(t)\,|n_1 n_2\rangle. \tag{A4}$$

Time evolution is governed by the effective non-Hermitian OPO Hamiltonian $H_{eff}$ (we use same notation as earlier sections)

$$|\Psi(t+\delta t) = (1 - iH_{eff}\delta t/\hbar)|\Psi(t)\rangle, \tag{A5}$$

where

$$H_{eff} = \frac{i\hbar}{2}p(a_1^{\dagger 2} - a_1^2) + \frac{i\hbar}{\sqrt{n_{\rm th}}}(a_1^{\dagger 2}a_2 - a_1^2 a_2^\dagger) - i\hbar\sum_{k=1}^{2} c_k^\dagger c_k, \tag{A6}$$

and the *collapse* operators are defined as

$$c_1 \equiv \sqrt{2}a_1 \quad \text{and} \quad c_2 \equiv \sqrt{2\gamma}a_2. \tag{A7}$$

The norm of the state operator is not preserved under time evolution

$$\langle\Psi(t+\delta t)|\Psi(t+\delta t)\rangle = \langle\Psi(t)|\Psi(t)\rangle - \delta P, \tag{A8}$$

where

$$\delta P = \sum_{k=1}^{2}\delta P_k \quad \text{and} \quad \delta P_k \equiv \delta t\,\langle\Psi(t)|c_k^\dagger c_k|\Psi(t)\rangle. \tag{A9}$$

Here $\delta P_1$, $\delta P_2$ are interpreted as the probabilities that the state vector will collapse with a photon being lost from the cavity subharmonic or pump mode, respectively. The time step $\delta t$ is adjusted so that $\delta P \ll 1$. A uniform random number $r_1$ is drawn at each time step and when $\delta P < r_1$, evolution proceeds as above for the next time step, while if $\delta P > r_1$, collapse occurs and a photon is lost into one of the two decay channels. Another uniform random number, $r_2$, is then selected to determine which channel is chosen. If $\delta P_1/\delta P > r_2$ the subharmonic decays by emitting a photon from the cavity; otherwise, the decay is via the pump mode; i.e., for $\delta P_1/\delta P > r_2$

$$|\Psi(t+\delta t)\rangle = \frac{c_1|\Psi(t)\rangle}{\sqrt{\delta P_1/\delta t}}, \tag{A10}$$

while for $\delta P_1/\delta P < r_2$ the subscripts 1 and 2 are interchanged in (A10).

A grid with size $N_1 = 32$ and $N_2 = 16$ was employed for the calculation of Fig. 9, large enough to ensure that boundary effects were negligible.


[1] B. Yurke, L. R. Corruccini, P. G. Kaminsky, L. W. Rupp, A. D. Smith, A. H. Silver, R. W. Simon, and E. A. Whittaker, Phys. Rev. A **39**, 2519 (1989).

[2] R. J. Thompson, G. Rempe, and H. J. Kimble, Phys. Rev. Lett. **68**, 1132 (1992).

[3] R. E. Slusher, Opt. Photon. News **4**, 8 (1993).

[4] Rüdiger Schack and Axel Schenzle, Phys. Rev. A **41**, 3847 (1990); F. Kärtner, R. Shack, and A. Schenzle, J. Mod. Opt. **39**, 917 (1992).

[5] A. M. Smith and C. W. Gardiner, Phys. Rev. A **39**, 3511 (1989).

[6] C. J. Mertens, T. A. B. Kennedy, and S. Swain, Phys. Rev. A **48**, 2374 (1993); Phys. Rev. Lett. **71**, 2014 (1993).

[7] C. J. Mertens and T. A. B. Kennedy, in *Quantum Optics VI*, edited by J. D. Harvey and D. F. Walls, Springer Proceedings in Physics Vol. 77 (Springer, New York, 1994).

[8] P. D. Drummond, K. J. McNeil, and D. F. Walls, Opt. Acta **28**, 211 (1981).

[9] K. Mølmer, Y. Castin, and J. Dalibard, J. Opt. Soc. Am. B **10**, 524 (1993).

[10] G. S. Agarwal, Phys. Rev. Lett. **73**, 552 (1994).

[11] C. M. Savage, Comput. Phys. **6**, 513 (1992).

[12] M. J. Collett and D. F. Walls, Phys. Rev. A **32**, 2887 (1985).

[13] L. I. Plimak and D. F. Walls, Phys. Rev. A **50**, 2627 (1994).

[14] Cyrano De Dominicis and Paul C. Martin, J. Math. Phys. **5**, 14 (1964).

[15] C. W. Gardiner and M. J. Collett, Phys. Rev. A **31**, 3761 (1985).

[16] H. R. Zaidi, Can. J. Phys. **66**, 854 (1988).

[17] P. Kinsler, Ph.D. thesis, University of Queensland, 1994 (unpublished).